A Letters Journal Exploring the Frontiers of Physics

February 2020

EPL, **129** (2020) 37002
doi: 10.1209/0295-5075/129/37002

www.epljournal.org

Magneto-transport in $La_{2/3}Sr_{1/3}MnO_3/YBa_2Cu_3O_7/Alq_3/Co$ spin-valves

Andrea Cerreta[1(a)], Roxana Gaina[1], Laura Nuccio[1], Ivan Marozau[1,2], Kaushik Sen[1,3], Roberto De Andrés Prada[1,4], Subhrangsu Sarkar[1] and Christian Bernhard[1(b)]

[1] *Physics Department and Fribourg Center for Nanomaterials (FriMat), University of Fribourg - Chemin du Musée 3, CH-1700 Fribourg, Switzerland*
[2] *CSEM SA - Rue Jaquet-Droz 1, CH-2002 Neuchâtel, Switzerland*
[3] *Institute for Solid State Physics, Karlsruhe Institute of Technology - D-76344 Eggenstein-Leopoldshafen, Germany*
[4] *Department of Physics, Stockholm University, AlbaNova University Center - SE-10691 Stockholm, Sweden*

received 13 December 2019; accepted in final form 7 February 2020
published online 26 February 2020

PACS 74.72.-h – Cuprate superconductors
PACS 74.25.-q – Properties of superconductors
PACS 72.25.-b – Spin polarized transport

Abstract – We studied how an additional layer of the high T_C superconductor YBCO affects the magneto-transport across a LSMO/Alq_3/Co spin-valve structure. We found that up to a thickness of at least 10 nm the YBCO layer on top of LSMO hardly changes the spin-valve effect, since the device resistance still depends on the relative orientation of the LSMO and Co magnetization. The spin-valve effect persists even when the superconducting YBCO layer acts as bottom electrode, with no spin-polarized current injected from LSMO into YBCO. This highlights that the charge carriers of a thin YBCO layer on top of LSMO are strongly spin-polarized, most likely due to a magnetic proximity effect involving a transfer of spin-polarized electrons from LSMO to YBCO. Evidence for a strongly underdoped state of the YBCO layers close to the interface with LSMO is indeed obtained from the dI/dV curves in zero magnetic field which reveal a pseudogap persisting well above T_C.

Introduction. – Spin-based electronics ("spintronics") utilizes the spin of the electrons in addition to their charge [1]. The most basic device is a so-called "spin-valve" that consists of two ferromagnetic electrodes with different coercive fields that are separated by a non-magnetic barrier. Its functionality relies on the transfer of spin-polarized charge carriers across the non-magnetic layer, such that the resistance depends on the relative orientation of the magnetisation of the ferromagnetic layers.

Most non-magnetic metals or semiconductors have a very short spin diffusion length that demands a very thin barrier of only few nanometers. So-called pinholes in the barrier due to the roughness of the layers are thus difficult to avoid unless sophisticated nano-fabrication tools are used to obtain a very small active area. Organic semiconductors provide much larger spin diffusion lengths and thus enable much thicker barrier layers (on the order of 100 nm). Functional devices with millimetre size active areas thus can be grown with simple shadow mask techniques [2].

The functionality of metal/organic spin-valves made from elemental ferromagnets, like Fe, Ni or Co (or permalloy) and thick ($d > 100$ nm) organic barriers from Alq_3, pentacene or rubrene has already been demonstrated [2]. Likewise, such spin-valves have been made using half-metallic perovskite $La_{2/3}Sr_{1/3}MnO_3$ (LSMO) as the ferromagnetic bottom electrode [2]. This raises expectations that one can incorporate other perovskite oxides or related layered materials, like cuprate high-T_C superconductors, whose exceptional electronic and magnetic properties may enable devices with strongly improved or new functionalities.

Superconductors are of particular interest due to their macroscopic quantum coherence and their loss-free and ultrafast response. For heterostructures from conventional

(a) E-mail: andrea.cerreta@outlook.com
(b) E-mail: christian.bernhard@unifr.ch

superconductors, like Nb, Pb or Al, and elemental ferromagnets, it has already been demonstrated that a spin-polarized superconducting state with spin-triplet Cooper-pairs can be achieved and utilized as source of spin-polarized supercurrents [3–7].

The research on corresponding heterostructures from oxide-based ferromagnets and cuprate high-T_C superconductors is comparably less advanced and conclusive, especially with respect to the superconducting spin-triplet state [8–12]. Nevertheless, it is meanwhile well established that an interesting magnetic proximity effect occurs in multilayers from $YBa_2Cu_3O_7$ (YBCO) and ferromagnetic manganites which gives rise to a ferromagnetic Cu moment on the YBCO side of the interface [13–16]. The mechanism underlying this proximity effect and the nature of the ferromagnetic Cu moments in YBCO, *e.g.*, whether they are localized or (at least partially) itinerant, remain to be determined. In terms of an itinerant picture, this proximity effect has been explained by a transfer of spin-polarized electrons from LSMO to YBCO that is driven by the work function difference [17–19]. Experimental evidence for such a transfer of electrons from the manganite to YBCO has been reported in refs. [20–23]. Moreover, there is evidence for a strong hybridisation of the interfacial Cu and Mn ions (along the interfacial Cu-O_{apical}-Mn bonds) which gives rise to an orbital reconstruction of the interfacial Cu ions and an antiferromagnetic exchange interaction that can also induce Cu moments [22–24] that are, however, likely bound to the interface. To our best knowledge there exists no direct measurement of the spin-polarization of the charge carriers at the cuprate/manganite interface and the length scale over which it persists away from the interface.

Here we provide this kind of information by studying the magneto-transport of spin-valve structures with a ferromagnetic bottom electrode from $La_{2/3}Sr_{1/3}MnO_3$ (LSMO), a layer of nominally optimally doped $YBa_2Cu_3O_7$ (YBCO), a non-magnetic layer from Alq_3 and a ferromagnetic Co top electrode. Our study provides evidence that the charge carriers in a YBCO layer on top of a ferromagnetic LSMO layer are spin-polarized over a length scale of at least 10 nm.

Materials and methods. – The devices were grown on insulating $10 \times 10 \times 0.5\,mm^3$ LSAT(001) crystal substrates. The multilayer structure (along the growth direction) consists of 60 nm of LSMO, 0 to 50 nm of YBCO, 140 nm Alq_3 and 10 nm Co. The cuprate and manganite layers were deposited with Pulsed Laser Deposition (PLD), while the Alq_3 and Co layers were grown with thermal evaporation. Shadow masks were used to define the typical geometry of these spin-valves as shown in fig. 1(a). The typical size of the active area for the perpendicular charge transport across the Alq_3 layer has the same lateral dimensions as the 4 mm diameter, circular Co layer, and therefore about $12.6\,mm^2$. The magneto-transport was measured in a Physical Property Measurement System (PPMS®, Quantum Design, Inc.) with the four-probe method. A remotely controlled Keithley 2602 System SourceMeter® was used to apply electrical signals (DC constant current or voltage) and collect data. As electrical contacts we glued thin copper wires with silver paste on the top of the LSMO, YBCO and Co layers. The different configurations for the transport measurement between the LSMO and Co (LSMO_Co), YBCO and Co (YBCO_Co), and the LSMO and YBCO (LSMO_YBCO) layers are detailed in fig. 1(b). For the magneto-resistance (MR) measurements the samples were zero-field–cooled and the magnetic field, H_{ext}, was parallel to the layers. More details about the sample preparation and techniques are given in the Supplementary Material `Supplementarymaterial.pdf` (SM).

Results. – Figure 1(c) displays a representative MR curve of a plain LSMO/Alq_3/Co spin-valve structure (SV) without any YBCO layer for the LSMO-Co configuration at 10 mV and $T = 10$ K. It reveals a typical spin-valve effect with a reduction (increase) of the resistance for an antiparallel (parallel) orientation of the magnetization of the LSMO and Co layers.

Figures 1(d) and (e) show the corresponding MR curves of the LSMO/YBCO/Alq_3/Co structures SV+Y_5 and SV+Y_10 with additional YBCO layers that are 5 and 10 nm thick, respectively. The superconducting transition of these YBCO layers is evident from a sudden drop in the *R-T* curves taken in LSMO-YBCO configuration, as shown in fig. 1(g) for the SV+Y_10 structure with $T_C \approx 65$ K (red line). The MR curves in figs. 1(d) and (e) were obtained in the LSMO-Co configuration at $T = 10$ K and applying 5 mV and 20 mV, respectively, and show for both structures clear spin-valve effects similar to the one of the plain SV structure in fig. 1(c). The spin-valve effect is even somewhat larger for the SV+Y_10 structure in fig. 1(e) than for SV+Y_5 in fig. 1(d). The more gradual and irreversible changes of the MR curve of SV+Y_10 seem to be caused by pinned vortices that arise from a small out-of-plane component of the magnetic field (due to an imperfect sample alignment).

The persistence of the spin-valve effect in these SV+Y_5 and SV+Y_10 structures suggests that the charge carriers of the thin YBCO layer on top of the ferromagnetic LSMO are spin-polarized. Furthermore, as shown in fig. 1(f), the MR curves of the SV+Y_10 structure exhibit a clear spin-valve effect even when they are taken with the YBCO-Co configuration at $10\,K \ll T_C \approx 65\,K$. Notably, in this configuration the LSMO layer is shorted by the superconducting YBCO layer, *i.e.*, there is no current flow through the LSMO layer and thus no injection of spin-polarized charge carriers from LSMO into YBCO is expected to take place. This highlights that the spin-polarization of the charge carriers of the YBCO layer occurs independently of the current-induced spin-injection from LSMO into YBCO. The spin-polarized charge carriers in YBCO thus seem to be induced by a permanent proximity effect

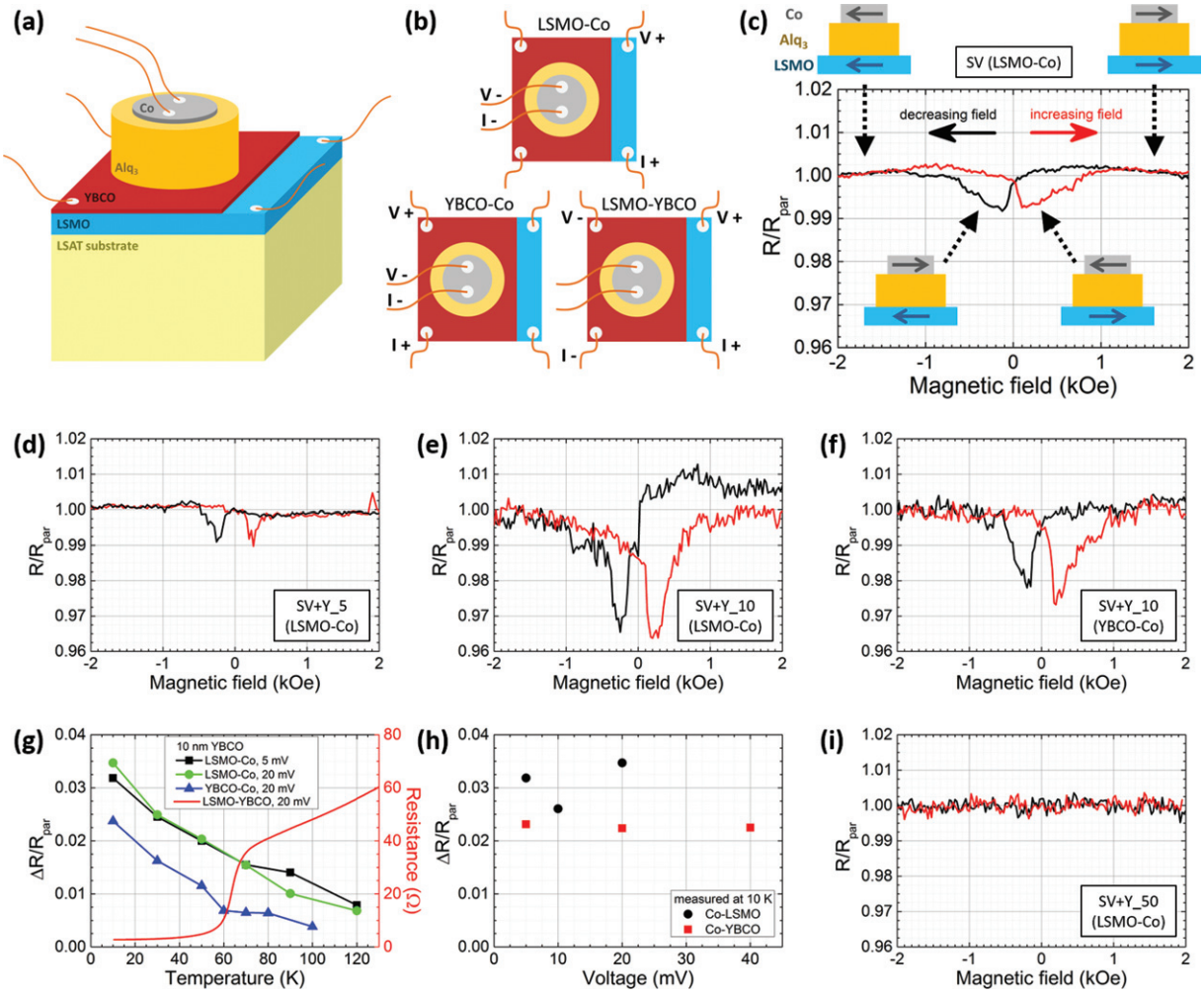

Fig. 1: (a) Typical geometry of the spin-valve devices. (b) Schemes of the different transport measurement configurations; contacts named $I+$ ("current in"), $I-$ ("current out"), $V+$ ("high voltage") and $V-$ ("low voltage") denote where voltage and current are applied or measured. In the LSMO-Co configuration (top image), the entire device is probed; in the YBCO-Co configuration (bottom left), the carriers are injected directly into YBCO bypassing LSMO, especially below T_C; in the LSMO-YBCO configuration (bottom right), only the two bottom layers are probed. (c) Normalized resistance *vs.* external magnetic field loop for a spin-valve (SV) without YBCO measured at 10 K with an applied voltage of $V0 = 10$ mV in the LSMO-Co configuration. The change of the relative orientation of the magnetic polarization of the Co and LSMO layers is sketched. (d) Normalized field loop of SV + 5 nm YBCO ($T = 10$ K, $V0 = 5$ mV, LSMO-Co configuration). (e) Normalized field loop of SV + 10 nm YBCO ($T = 10$ K, $V0 = 20$ mV, LSMO-Co configuration). (f) Same SV and conditions as in (e), but for the YBCO-Co configuration. (g) Temperature dependence of the normalized magneto-resistance ΔR for SV + 10 nm YBCO. Data acquired at $V0 = 5$ and 20 mV and in different contact configurations are compared. In the same graph, the R-T curve in LSMO-YBCO configuration shows the SC transition at $T_C \approx 65$ K. (h) Normalized ΔR *vs.* $V0$ at 10 K for SV + 10 nm YBCO in different configurations. (i) Normalized loop for a SV+50 nm YBCO ($T = 10$ K, LSMO-Co configuration) which shows no spin-valve effect.

at the interface between the YBCO and the FM LSMO layers (as discussed in the introduction).

Figure 1(g) compares the magnitude of the spin-valve effect for the different structures and contact configurations and shows that they exhibit similar temperature dependences with a continuous increase toward low temperature. The temperature dependence resembles the one of the plain $LSMO/Alq_3/Co$ structures where it was explained in terms of an increase of the spin-diffusion length of the Alq_3 layer [25]. This suggests that the onset of superconductivity in the YBCO layer does not strongly influence the spin-valve effect. This conclusion is corroborated by the data in fig. 1(h) which reveal that the spin-valve effect hardly depends on the applied voltage, *i.e.*, whether it is smaller or larger than the superconducting energy gap of YBCO of $\Delta_{SC} \approx 19$ meV (see refs. [26,27] and the discussion below). Finally, fig. 1(i) shows that the spin-valve effect is absent (within the noise level) for the structure with a 50 nm thick YBCO layer. In the SM it is furthermore shown that no spin-valve effect occurs for a corresponding $YBCO(10\,nm)/Alq_3/Co$ structure with $T_C \approx 76$ K that has no LSMO layer.

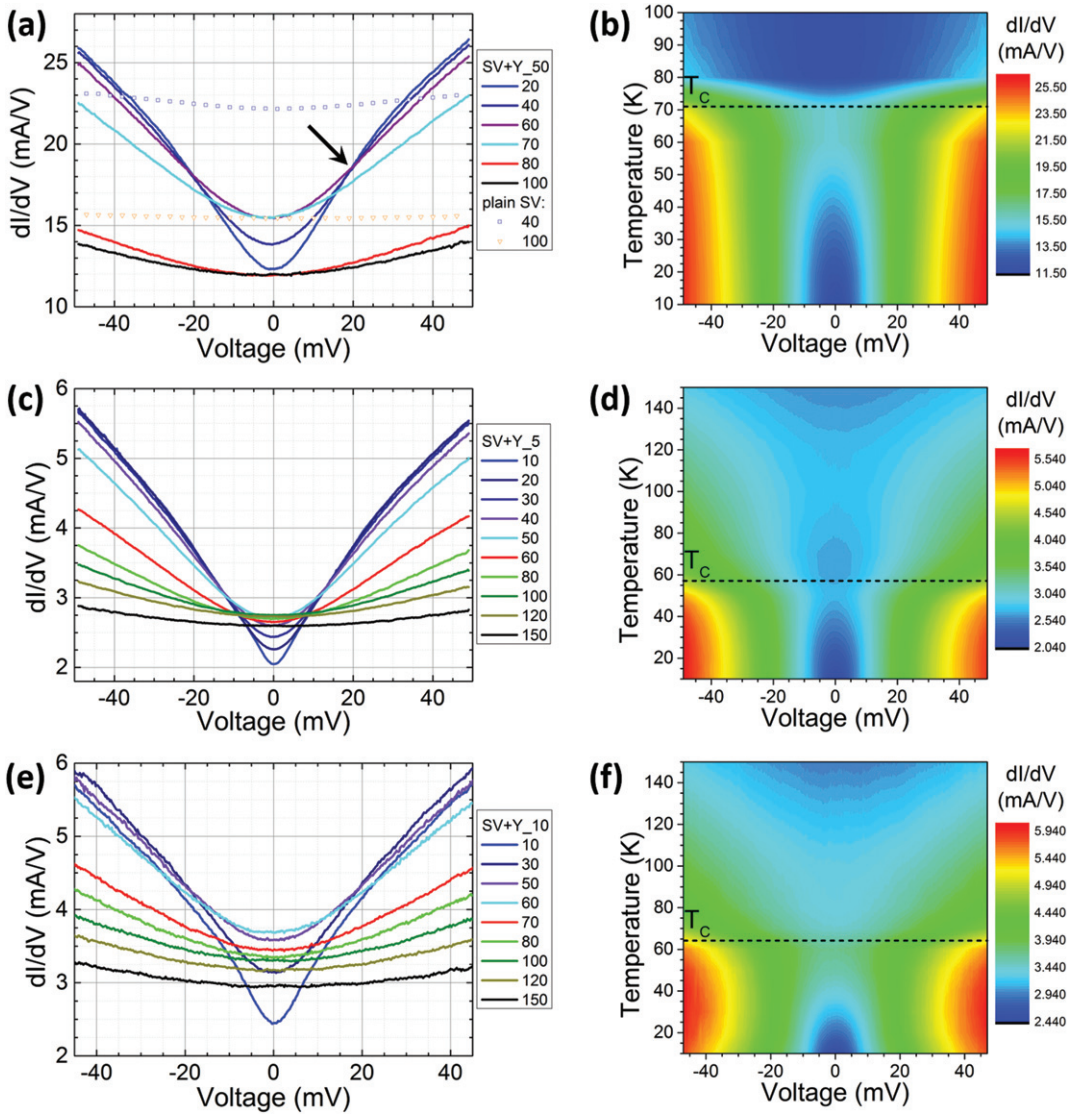

Fig. 2: (a) dI/dV *vs.* voltage curves at different temperatures measured on SV+50 nm YBCO (LSMO-Co configuration); results at selected temperatures are compared to those for a SV without YBCO. (b) 2D color map of dI/dV *vs.* temperature and voltage on the same SV+50 nm YBCO (LSMO-Co configuration); the dashed line indicates T_C. (c) and (d): selected dI/dV *vs.* voltage curves at different temperatures and 2D color map for SV+5 nm YBCO. (e) and (f): The same as before for SV+10 nm YBCO.

Next, we focus on the corresponding dI/dV curves in zero magnetic field, which reveal the signatures of a superconducting gap formation below T_C and of a pseudogap that persists well above T_C. This confirms that these transport experiments are sensitive to the electronic and superconducting properties of the YBCO layer, *i.e.*, they are not governed by defects within the YBCO layer at which superconductivity is suppressed. The coincidence of the pseudogap in the dI/dV curves and the spin-valve effect in the MR-curves for SV+Y_5 and SV+Y_10 is also in line with the scenario of a transfer of spin-polarized electrons from LSMO to YBCO for which the latter becomes strongly underdoped.

Discussion. – We start with the discussion of the dI/dV curves of the SV+Y_50 structure that does not exhibit a spin-valve effect. Representative dI/dV curves below and above $T_C \approx 72$ K are shown in fig. 2(a), more data are displayed in terms of a 2D contour plot in fig. 2(b). They reveal that the dI/dV curves undergo rather sudden changes between 70 K and 80 K that are characteristic of the opening of a superconducting gap. The dI/dV curves in the normal state between 100 and 80 K are only weakly voltage-dependent and rather similar, whereas the dI/dV curve at 70 K is already upward shifted and has a much larger curvature. The curvature keeps increasing for the curves at $T \leq 60$ K which develop additional features in terms of a sharper minimum around zero bias and a kink in the slope that eventually gives rise to a crossing point around 19(1) meV. The latter is indeed close to the superconducting energy gap of $\Delta_{SC} \approx 18$ meV as reported from a scanning tunneling spectroscopy (STS)

study of YBCO [26]. That the dI/dV curves in fig. 2(a) and (b) do not exhibit the superconducting coherence peak seen in STS [26,27] can be understood in terms of disorder effects due to the millimeter-sized active area of our device and the large thickness of our Alq_3 barrier. Accordingly, we assign this combined kink feature and crossing point to a superconducting gap of $\Delta_{SC} = 19(1)$ meV. For comparison, we also show by the open symbols in fig. 2(a) the dI/dV curves of a plain SV. They are almost flat and featureless and confirm our interpretation of the above discussed structures in terms of the superconducting gap of YBCO.

We proceed to the dI/dV curves and the contour plots for the corresponding spin-valve structures with 5 nm and 10 nm of YBCO in figs. 2(c) and (d) and figs. 2(e) and (f), respectively. Below $T_C \approx 58$ K and $T_C \approx 65$ K they reveal similar gap features with a sharp minimum around zero bias and kinks and crossing points near 12 meV for SV+Y_5, between 16 and 21 mV for SV+Y_10. The most remarkable difference concerns the behavior at $T \geq T_C$, where the signatures of the gap disappear much more gradually than for SV+Y_50 and persist well above 100 K. This behavior is characteristic of the pseudogap phenomenon that is observed in the tunneling spectra of strongly underdoped cuprates [27]. The circumstance that these structures also exhibit the spin-valve effect in the MR-curves (see fig. 1(d) and (e)) finds a natural explanation in terms of a transfer of spin-polarized electrons from LSMO to YBCO as discussed in the introduction. Note that an additional contribution to an overall reduced hole doping of all the YBCO layers (not only in the vicinity of the YBCO/LSMO interface) may arise from oxygen vacancies that develop during the Co deposition, which can lead to a moderate sample heating and thus oxygen diffusion. Apart from other defects and finite-size effects, this would explain the fairly low T_C values (as compared to optimally doped, bulk YBCO with $T_C \approx 90$ K) of the spin-valve with 50 nm of YBCO in fig. 2(a) and (b) and of the YBCO(10 nm)/Alq_3/Co structure without a LSMO layer in the SM. Accordingly, the charge transfer at the YBCO/LSMO interface would drive the CuO_2 layers in the vicinity of the interface from a weakly to a more strongly underdoped state.

Conclusions. – To conclude, we studied how the spin-dependent transport across a LSMO/Alq_3/Co spin-valve structure is modified by an additional YBCO layer between LSMO and Alq_3. We found that up to a thickness of 10 nm the YBCO becomes strongly spin-polarized such that a sizeable spin-valve effect occurs even if the superconducting YBCO layer serves as bottom electrode. Notably, the superconducting transition of the YBCO layer hardly influences this spin-valve effect. This does not exclude a possible spin-triplet component of the condensate that could only be probed for structures with much thinner barriers that allow one to maintain the superconducting phase coherence. It suggests, however, that the spin-polarized charge carriers of this YBCO layer are not directly involved in the formation of the superconducting condensate. For the bulk cuprate high-T_C superconductors it is indeed well established, *e.g.*, from tunneling and infrared spectroscopy [26,28–30], that a large fraction of the charge carriers remains unpaired and are subject to other kinds of correlation or ordering phenomena, for example related to the charge-density-wave (CDW), spin-density-wave (SDW) or stripe phases that are currently under intense investigation [31]. It is well known that these competing correlations get most pronounced in the strongly underdoped regime where a so-called pseudogap develops well above T_C. Our observation of a coincidence of this pseudogap phenomenon with the strong spin-polarization of the charge carriers in a thin YBCO layer in proximity to ferromagnetic LSMO thus adds another interesting facet to the fascinating spectrum of physical phenomena that emerge from the competing orders in these strongly correlated materials.

* * *

The work at the University of Fribourg was supported by the Schweizer Nationalfonds (SNF) through grants Nos. 200020-172611 and CRSII2-154410/1.

REFERENCES

[1] Wolf S. A., Awschalom D. D., Buhrman R. A., Daughton J. M., von Molnár S., Roukes M. L., Chtchelkanova A. Y. and Treger D. M., *Science*, **294** (2001) 1488.
[2] Dediu V. A., Hueso L. E., Bergenti I. and Taliani C., *Nat. Mater.*, **8** (2009) 707.
[3] Buzdin A., *Nat. Mater.*, **3** (2004) 751.
[4] Linder J. and Robinson J. W. A., *Nat. Phys.*, **11** (2015) 307.
[5] Robinson J. W. A., Witt J. D. S. and Blamire M. G., *Science*, **329** (2010) 59.
[6] Khaire T. S., Khasawneh M. A., Pratt W. P. jr. and Birge N. O., *Phys. Rev. Lett.*, **104** (2010) 137002.
[7] Eschrig M., *Phys. Today*, **64** (2011) 43.
[8] Dybko K., Werner-Malento K., Aleshkevych P., Wojcik M., Sawicki M. and Przyslupski P., *Phys. Rev. B*, **80** (2009) 144504.
[9] Kalcheim Y., Kirzhner T., Koren G. and Millo O., *Phys. Rev. B*, **83** (2011) 064510.
[10] Visani C., Sefrioui Z., Tornos J., Leon C., Briatico J., Bibes M., Barthélémy A., Santamaría J. and Villegas J. E., *Nat. Phys.*, **8** (2012) 539.
[11] Golod T., Rydh A., Krasnov V. M., Marozau I., Uribe-Laverde M. A., Satapathy D. K., Wagner T. and Bernhard C., *Phys. Rev. B*, **87** (2013) 134520.
[12] Egilmez M., Robinson J. W. A., MacManus-Driscoll J. L., Chen L., Wang H. and Blamire M. G., *EPL*, **106** (2014) 37003.
[13] Stahn J., Chakhalian J., Niedermayer Ch., Hoppler J., Gutberlet T., Voigt J., Treubel F.,

Habermeier H.-U., Cristiani G., Keimer B. and Bernhard C., *Phys. Rev. B*, **71** (2005) 140509(R).

[14] Chakhalian J., Freeland J. W., Srajer G., Strempfer J., Khaliullin G., Cezar J. C., Charlton T., Dalgliesh R., Bernhard C., Cristiani G., Habermeier H.-U. and Keimer B., *Nat. Phys.*, **2** (2006) 244.

[15] Satapathy D. K., Uribe-Laverde M. A., Marozau I., Malik V. K., Das S., Wagner Th., Marcelot C., Stahn J., Brück S., Rühm A., Macke S., Tietze T., Goering E., Frañó A., Kim J.-H., Wu M., Benckiser E., Keimer B., Devishvili A., Toperverg B. P., Merz M., Nagel P., Schüppler S. and Bernhard C., *Phys. Rev. Lett.*, **108** (2012) 197201.

[16] Alberca A., Uribe-Laverde M. A., Windsor Y. W., Ramakrishnan M., Rettig L., Marozau I., Tonnerre J.-M., Stahn J., Staub U. and Bernhard C., *Phys. Rev. B*, **92** (2015) 174415.

[17] Yunoki S., Moreo A., Dagotto E., Okamoto S., Kancharla S. S. and Fujimori A., *Phys. Rev. B*, **76** (2007) 064532.

[18] Yang X., Yaresko A. N., Antonov V. N. and Andersen O. K., arXiv:0911.4349.

[19] Salafranca J., Rincón J., Tornos J., León C., Santamaria J., Dagotto E., Pennycook S. J. and Varela M., *Phys. Rev. Lett.*, **112** (2014) 196802.

[20] Holden T., Habermeier H.-U., Cristiani G., Golnik A., Boris A., Pimenov A., Humlíček J., Lebedev O. I., Van Tendeloo G., Keimer B. and Bernhard C., *Phys. Rev. B*, **69** (2004) 064505.

[21] Varela M., Lupini A. R., Pennycook S. J., Sefrioui Z. and Santamaria J., *Solid-State Electron.*, **47** (2003) 2245.

[22] Chakhalian J., Freeland J. W., Habermeier H.-U., Cristiani G., Khaliullin G., Van Veenendaal M. and Keimer B., *Science*, **318** (2007) 1114.

[23] Seo A., Boris A. V., Cristiani G., Habermeier H.-U. and Keimer B., *Phys. Rev. B*, **99** (2019) 064501.

[24] Sen K., Perret E., Alberca A., Uribe-Laverde M. A., Marozau I., Yazdi-Rizi M., Mallett B. P. P., Marsik P., Piamonteze C., Khaydukov Y., Döbeli M., Keller T., Biškup N., Varela M., Vašátko J., Munzar D. and Bernhard C., *Phys. Rev. B*, **93** (2016) 205131.

[25] Drew A. J., Hoppler J., Schulz L., Pratt F. L., Desai P., Shakya P., Kreouzis T., Gillin W. P., Suter A., Morley N. A., Malik V. K., Dubroka A., Kim K. W., Bouyanfif H., Bourqui F., Bernhard C., Scheuermann R., Nieuwenhuys G. J., Prokscha T. and Morenzoni E., *Nat. Mater.* **8** (2009) 109.

[26] Bruér J., Maggio-Aprile I., Jenkins N., Ristić Z., Erb A., Berthod C., Fischer Ø. and Renner C., *Nat. Commun.*, **7** (2016) 11139.

[27] Fischer Ø., Kugler M., Maggio-Aprile I., Berthod C. and Renner C., *Rev. Mod. Phys.*, **79** (2007) 53.

[28] Tanner D. B., Liu H. L., Quijada M. A., Zibold A. M., Berger H., Kelley R. J., Onellion M., Chou F. C., Johnston D. C., Rice J. P., Ginsberg D. M. and Markert J. T., *Physica B*, **244** (1998) 1.

[29] Tajima S., Kakeshita T., Fudamoto Y., Wang N. L., Železný V., Kojima K. M., Uchida S., Gorshunov B. and Dressel M., *J. Phys. Chem. Solids* **67** (2006) 321.

[30] Liu H. L., Quijada M., Romero D. B., Tanner D. B., Zibold A., Carr G. L., Berger H., Forró L., Mihaly L., Cao G., O B.-H., Markert J. T., Rice J. P., Burns M. J. and Delin K. A., *Ann. Phys.*, **15** (2006) 606.

[31] Keimer B., Kivelson S. A., Norman M. R., Uchida S. and Zaanen J., *Nature*, **518** (2015) 179.